Research Article Vol. 29, No. 2 / 18 January 2021 / Optics Express 2521
Optics EXPRESS

Neural network enabled metasurface design for phase manipulation

LI JIANG,[1,3] XIAOZHONG LI,[2,3] QINGXIN WU,[1] LIANHUI WANG,[1] AND LI GAO[1,4]

[1]*Key Laboratory for Organic Electronics and Information Displays (KLOEID), Institute of Advanced Materials (IAM), School of Materials Science and Engineering, Nanjing University of Posts and Telecommunications, Nanjing 210023, China*
[2]*School of Electronic and Optical Engineering, Nanjing University of Science and Technology, Nanjing 210094, China*
[3]*These authors contributed equally*
[4]*iamlgao@njupt.edu.cn*

Abstract: The phase of electromagnetic waves can be manipulated and tailored by artificial metasurfaces, which can lead to ultra-compact, high-performance metalens, holographic and imaging devices etc. Usually, nanostructured metasurfaces are associated with a large number of geometric parameters, and the multi-parameter optimization for phase design cannot be possibly achieved by conventional time-consuming simulations. Deep learning tools capable of acquiring the relationship between complex nanostructure geometry and electromagnetic responses are best suited for such challenging task. In this work, by innovations in the training methods, we demonstrate that deep neural network can handle six geometric parameters for accurately predicting the phase value, and for the first time, perform direct inverse design of metasurfaces for on-demand phase requirement. In order to satisfy the achromatic metalens design requirements, we also demonstrate simultaneous phase and group delay prediction for near-zero group delay dispersion. Our results suggest significantly improved design capability of complex metasurfaces with the aid of deep learning tools.

1. Introduction

Metasurface is a planar nanostructured surface that strongly interacts with electromagnetic (EM) wave and shapes the wavefront property [1]. The pioneer work of generalized Snell's law of refraction has inspired intensive research on function-specific metasurfaces [1,2], which lead to ultra-compact, nanoscale optical devices, including metalenses [3–10], camera [11–13], spectral filtering [14], electromagnetic enhancement [15,16], holograms [17,18] and so on. Among them, nanofin is a type of metasurfaces that can control the phase of light for obtaining broadband achromatic and even polarization-insensitive metalens imaging [3,5,6]. In previous practice, a library that contains thousands of phase values can be generated by simulating thousands of different nanofin structures. Optimization tool is then used to search for the closest phase values in the library to satisfy the metalens design requirements by arranging the spatial distributed cells. However, this small library only provides very limited phase choices, as a result, the metalens size is limited to only tens of micrometers with coarse design accuracy. If we want to design larger metalens with better accuracy, we need to build geometry-property library with much denser data points. Taking a typical TiO_2 nanofin unit cell plotted in Fig. 1(a) as an example, by fixing the gap and thickness parameter, six lateral geometric parameters all affect the EM responses and can easily exceed millions of different combinations. Such enormous amount of data will take tens of years' time to generate by full-wave simulation tools, and more importantly, there is no efficient optimization tool to search such gigantic space for globally optimized results that satisfy on-demand applications.

#413079 https://doi.org/10.1364/OE.413079
Journal © 2021 Received 23 Oct 2020; revised 13 Dec 2020; accepted 30 Dec 2020; published 14 Jan 2021

Optics EXPRESS

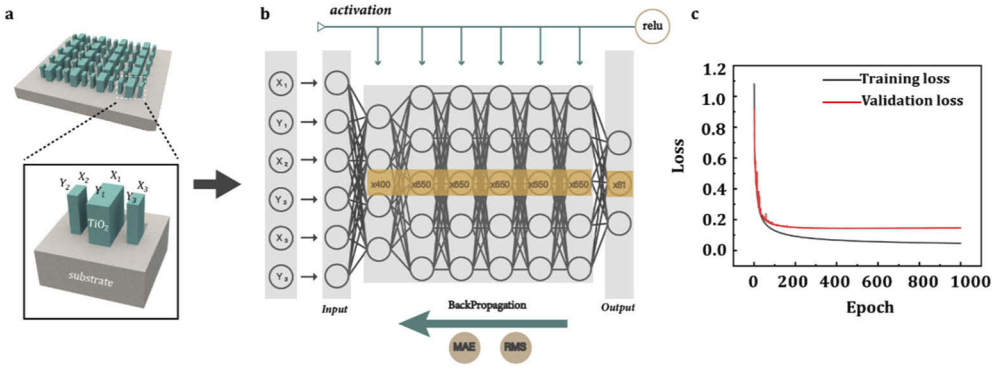

Fig. 1. Illustration of the metasurface design, DNN and loss curves. (a) Metasurface schematic composed of three nanofin structures and six lateral geometric parameters. (b) The architecture of DNN where the input layer is geometric parameters and the output layer is the phase response. (c) The training loss and validation loss of DNN.

Machine learning is a data-driven approach which can learn the hidden relationship between data structures [19–21]. Neural network architectures such as generative adversarial network [22], convolutional neural network [23] and semi-supervised learning strategy [24] can be selected for specific problems. The power of machine learning has revolutionized our capability to process, comprehend and apply data. In the field of nanophotonics, deep neural network (DNN) is best suited for investigating regularly shaped nanostructure with multiple geometric parameters. By providing adequate training data, DNN can accurately capture the complex relationship between nanostructure geometry and EM response, which helps us to better understand light-matter interactions. It can replace or complement conventional simulation with orders of magnitude faster speed, and enable direct inverse design of nanostructures based on desired EM response which cannot be completed by numerical optimizations. Typical applications include transmission/reflection spectra [22–29], magnetic response [30,31] and structural colors [32] generated by dielectric metasurfaces and metallic plasmonics.

However, the design of metasurface for phase manipulation remains a great challenge for DNN training, since phase values are one type of complex data structure that experiences phase discontinuity of 180° at resonant wavelengths, and such abrupt change is affected by all the geometric parameters of the nanofin structure. Previous DNN training can only deal with simple data structure such as resonance amplitude that has smooth data distribution in the range between 0 to 1. Recent efforts used two individual networks to predict the real and imaginary part of transmission coefficients, and retrieve the phase response by subsequent calculations, which ingeniously avoid the direct training of phase [29]. The results show excellent consistency between simulations and predicted response. However, training of two individual networks and the subsequent calculating procedure means lower efficiency and increased complexity. To perform inverse design, the two separate networks need to use the same inputs while having their respective losses and gradients. This may cause conflict during the optimization that prevents inverse design of phase. Therefore, direct manipulation and training of phase data becomes necessary. An inverse phase design model for nanocylinder metasurface attempts to design just a single parameter of radius by fixing the height value, where simultaneous inverse design of multiple geometric parameters is not yet realized [33]. Moreover, previous DNN only handles geometric parameters that are less than four, whether DNN can handle more parameters and train complex abrupt phase data remains a question. Here, we use nanofin shown in Fig. 1(a) as an ideal platform to test DNN's capability to deal with six-dimensional parameter training and optimization, our results show that by carefully building the network architecture and optimize

Optics EXPRESS

the training methods, accurate phase prediction and complex metasurface inverse design can be performed to satisfy on-demand phase requirements. The network and design procedures are much simplified compared to previous efforts, since the direct prediction of phase response with one single network is realized. We drop the intricate neural tensor network (NTN) layer used in Ref. [29] because the training time would greatly expand when size of datasets increases to hundreds of thousands. Results show that accurate predictions of our single network are achieved as well.

2. Results

In this work, finite difference time domain (FDTD) method is used to obtain 7680 groups of phase data for different parameter combinations. The complete phase spectra are composed of 81 frequency points uniformly distributed among wavelength of 380 nm ~ 780 nm with the interval of 5 nm. The inaccuracy of phase prediction, by analyzing, generally happens when sparse samples are distributed around the phase shifts, where some features are missed. We demonstrate two classical situations in Supplement 1, Fig. S1. Thus, the sampling interval here is determined by a quantity of tests to ensure a fine coverage of the phase shifts features, so that the discontinuity can be learned by the DNN method. Phase responses of each wavelength are acquired by the transmission coefficients in the S-matrix during the simulation. The length and width of the three nanofins are varied to ensure sufficient phase value distributions. As shown in Fig. 1(a), the input of the network are six geometric parameters of the nanofin and the output are the corresponding phase values at 81 different wavelengths. Six hidden layers are added in the DNN, which are made of 400, 650, 650, 650, 650,650 neurons, respectively. The datasets are split randomly before training, among which 680 groups of data are separated as validation datasets, and 100 groups of data are test groups. These data are not involved in training and later used as judgement of the DNN's performance, while all the rest of data groups are employed to train the DNN. The basic architecture of the DNN shown in Fig. 1(b) is established by the Tensorflow and Keras frame to handle the regression problem between nanostructure parameters and phase spectra, for realizing the phase prediction of arbitrary structures. The geometric parameters are preprocessed by the normalization method of minmax_scale, which linearly rescale the parameters into a range of (0,1) so that eliminated the numerical difference between different parameters. Meanwhile, the loss function of mean absolute error (MAE) is chosen rather than the commonly used mean squared error (MSE) according to the practical performance of the DNN (The loss calculation method can be seen in method section). Then Root Mean Squared Propagation (RMSProp) optimizer is applied to realize the backpropagation and update of the weights. This algorithm can reduce the oscillation and avoid the noise caused by the dominating signal. Other hyperparameters like batch size, learning rate, learning rate decay, epoch number etc. are also constantly adjusted to optimize the training process and ensure better performances of the DNN, which can be reflected by the training and validation loss values. Optimal DNN architecture setting is shown in Supplement 1, Table S1 and comparison of some hyperparameters are plotted as loss in Supplement 1, Fig. S2. Figure 1(c) shows the loss curves of the training process, which converge to a constant value after 200 epochs, and it indicates the network is trained effectively. The training is completed when the loss reaches the predetermined value or iterative calculation ends.

Unlike previous methods that predict the phase response by calculating the real and imaginary parts of the transmission coefficient [29], our DNN can directly predict the phase response of any nanofin structures. Figures 2(a)–2(c) shows representative broadband phase spectra of three randomly selected structures in the test datasets. The prediction errors of the total 100 test groups are plotted in Fig. 2(d) (error calculation methods can be seen in the method section of Supplement 1) with averaged error of 0.076. The embedded histogram shows statistics of the errors, with 74 samples have errors less than the average, 17 samples have errors between 0.076

Optics EXPRESS

and 0.2, and 7 samples have errors larger than 0.2. Additional DNN predicted phase spectra results are displayed in Supplement 1, Figs. S3 and S4. Figures 2(e)–2(g) shows that different nanofin structures can generate 2π phase response at three specific wavelengths of 420 nm, 495 nm and 735 nm. It is observed that one sample in the test data exhibits much higher error than any other samples, and the comparison of phase spectrum is shown in Fig. 2(h). By analysis the spectrum has more phase jumps than usual case and the drastic shift may be responsible for the inferior prediction. At every drastic phase shift, very little offset of the points will result in large errors, but such problem can be eased by more dense sampling points of the simulated phase spectra.

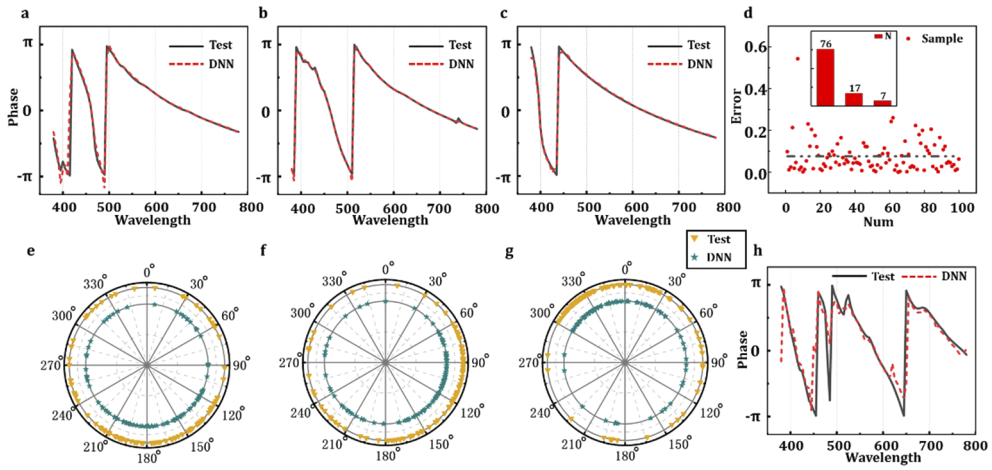

Fig. 2. Representative DNN prediction results of phase responses. (a-c) Three phase spectra predicted by DNN with pre-known nanofin geometry (test data group No. 3, 25 and 31 with details shown in Supplement 1, Table S2). (d) Predicting error distribution of the total 100 test group, with an average error value of 0.076. Statistics show that 76 of the 100 samples is below the average and 93% samples have an error less than 0.2. (e-g) 2π phase prediction by DNN at wavelengths of 420 nm, 495 nm and 735 nm. (h) The phase spectra predicted by DNN with largest error of 0.56 (test data group No. 7).

For the first time, we also use DNN to realize the inverse design of the nanofin metasurfaces that satisfy on-demand phase responses. Weights of the well-trained DNN are reused in the inverse network. The input geometric parameters are initialized as constants before the design, and loss of the output phase and actual phase is calculated to update the initialized geometric parameters. The optimization continues until the loss is small enough, which means that the predicted phase of the designed structure is close to the actual values. Structures designed by the network are then simulated by the FDTD method to get the phase response for comparison. The inverse design here is challenging due to six geometric parameters are involved while previous inverse designs only deal with three or four parameters. In our case, six parameters would generate various parameter combinations that all satisfy the DNN's prediction. The mechanism of DNN training determines that although the network can accept any input parameters, but only parameters covered by or close to training datasets give excellent predictions. The farther input parameters deviate from the training datasets range, the poorer results would be. In extreme cases, negative values which are completely unreasonable will also be misjudged as correct by the DNN, because the wrong parameter combination may also output the same results with simple numerical calculation by weights. This situation seldom appears when inputs are simple data structures that have uncomplicated mapping relation and optimal direction. However, with increasing number of the input parameters, possible combinations grow exponentially and choice

Optics EXPRESS

of optimal direction also becomes diverse, making the design extremely challenging. This would not cause troubles in the forward process because unreasonable parameters will not be input into the NN, but it affects in the inverse process as the geometric parameters are optimized by the DNN and the results can deviate from regular parameter space.

Two corresponding measures are taken to overcome these difficulties. Firstly, a sigmoid function is inserted between the input and first hidden layer, which can also be seen as the active function, but it connects directly after the input. This nonlinear function can turn the input parameters to numbers between 0 and 1, which is the normal range of datasets. If we take the original input as x_0, the input after the sigmoid function is denoted as x. DNN would optimize x_0 based on the losses and reasonable corrections of x_0 within the normal range will be delivered to . But when x_0 is optimized to an unreasonable range, it will be greatly compressed by the sigmoid function and x will be adjusted back to the normal range after the sigmoid function. In the end, x rather than x_0 is adopted as the designed input values. This can guarantee a correct inverse design result. Secondly, parameter combinations would provide various design results by any different settings of the DNN. In terms of this issue, we sweep the changeable hyperparameters of the DNN and record the loss values, and finally choose the minimum loss as the optimal designed result. Figures 3(a)–3(c) compare the inverse designed phase spectra of three nanofin structures and their true values. Similarly, we also calculate the errors of the test groups in Fig. 3(d) with embedded statistics. The average error of the 100 samples is 0.076, and 99% of the samples have errors less than 0.2. Surprisingly, the performance of inverse design is even better than that of forward network, which shows that we have accurately designed nanofin structures for on-demand phase requirements. Again, Figs. 3(d)–3(f) demonstrates the 2π phase coverage by inverse design at specific wavelengths. Additional DNN designed phase spectra results are displayed in Supplement 1, Figs. S5 and S6. The only one sample that turns out to have a poor design is shown in Fig. 3(h), with an error of 0.42. The network fails to meet the last peak and some small tips in the spectrum, but general trends are realized.

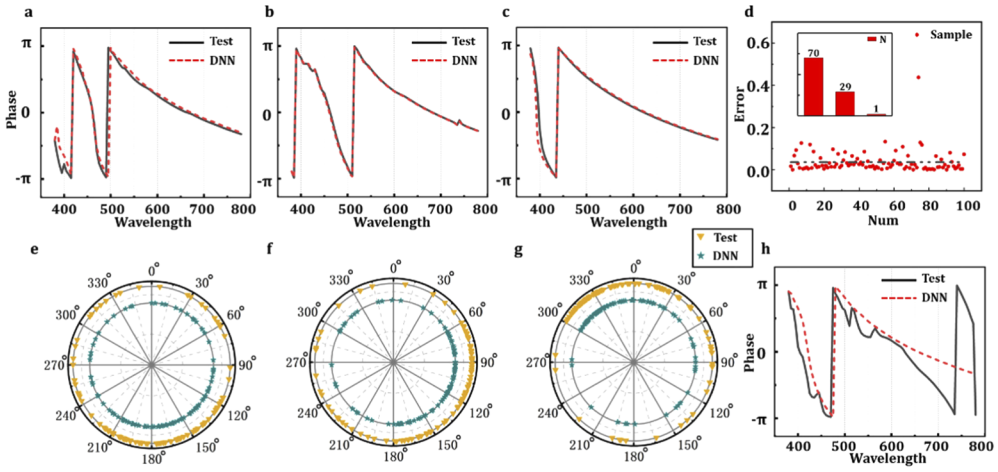

Fig. 3. Representative DNN inverse design results of phase responses. (a-c) Three phase spectra designed by DNN with comparison to the original data (test data group No. 3, 25 and 31). (d) Inverse designs' error distribution of the total 100 test group, with an average error value of 0.036. Statistics show that 70 of the 100 samples is below the average and 99% samples have an error less than 0.2. (e-g) 2π phase designed by DNN at wavelengths of 420 nm, 495 nm and 735 nm. (h) The phase spectra designed by DNN with largest error of 0.42(test data group No. 74).

Optics EXPRESS

To further demonstrate the power of DNN-based metasurface designs, we take the broadband achromatic metalens as an example to demonstrate accurate and simultaneous prediction of multiple phase properties. The design of achromatic metalens needs an accurate phase matching to achieve wavefront shaping of light. A phase profile for the metalens with focal length F can be formulated as:

$$\varphi(\mathrm{r},\omega) = -\frac{\omega}{c}\left(\sqrt{r^2+F^2}-F\right)$$

where c represents light speed, and phase varies with different radius r and angular frequency ω. Furtherly, the design of broadband achromatic metalens, as shown in previous work [5,6], still needs the manipulation of the higher-order derivative terms which determine the metalens dispersion. That is, a simultaneous accurate match of phase and group delay (GD) values at specific wavelengths, while keeping group delay dispersion (GDD) value close to zero, to achieve achromatic phase manipulation over a metalens surface for a broad range of wavelength. The phase profile forms a spherical wavefront and group delay (GD) compensates for the difference in the wavepackets' arrival times at the focus. Higher-order derivative terms like group delay dispersion (GDD) ensure that the outgoing wavepackets are identical. The phase and GD profile can be realized by the nanofin structure with DNN method applied above, which has exhibited the 2π phase coverage for different wavelengths. Libraries built by EM simulated phase properties were used to search the most proper structures for metalens before. The network here needs to realize the accurate prediction of phase and GD response of different nanofin structures at every single wavelength, which can help to choose the structures for metalens.

In order to train such network, we split the phase spectra at every single wavelength to calculate the corresponding GD and GDD values. Here, we calculate GD and GDD values based on Eq. (8) in the method section. 622080 groups of data are obtained as each phase spectrum can be split to 81 groups corresponding to the 81 points of wavelength, and 69734 of them with GDD values close to 0 are screened out as datasets for training the DNN. Such training datasets are set

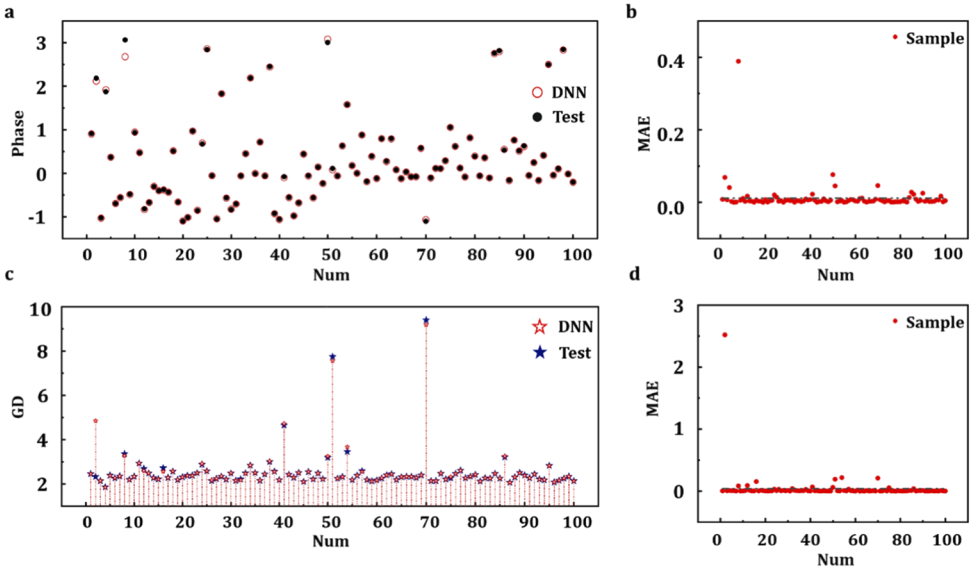

Fig. 4. Simultaneous prediction results of phase and group delay values, with precondition of near-zero group delay dispersion. (a) Phase prediction results compared with true values and (b) the error calculation of test datasets. (c) Group delay prediction results compared with true values and (d) the error calculation of test datasets. The average error shown in b and d are 0.0428 and 0.0117, respectively.

Optics EXPRESS

up to realize all possible predictions of phase and GD values at the precondition of near-zero GDD. Among them 6634 groups are separated to serve as the validation group, and another 100 groups are randomly selected to test the network. Input layer of the DNN contained the same six geometric parameters and an extra wavelength parameter, and output layer consists of the phase and GD values. The training process shows smooth convergence after hundreds of epochs. We then employ the test data and plotted the predicted results in Figs. 4(a), 4(c). One hundred groups of phase and GD values are compared with the true value in the graph. Solid graphics represent test datasets, while hollow shapes are the predicted data. It can be seen that predictions are very accurate with very few exceptions. At the same time, the absolute errors shown in Figs. 4(b), 4(d) also indicate that the simultaneous phase and GD prediction is very accurate. With the well-trained DNN based on less than seventy thousand datasets, we can easily output millions of corresponding phase and GD values while keeping GDD close to zero. Such tool can build a complete phase and GD library for achromatic phase designs, which is much more effective than building data libraries through EM simulations.

3. Conclusion

In this work, by inserting a sigmoid function between the input and first hidden layer, taking MAE as the loss function and carefully optimizing hyperparameter settings, for the first time, we report direct DNN training of six geometric parameters and abrupt phase change data. The results show both accurate forward prediction and inverse design of nanofin metasurfaces for phase manipulation. Such DNN method can also be applied in achromatic metalens designs, where countless phase and group delay values can be obtained effortlessly while keeping the group delay dispersion value close to zero. Our model suggests enhanced functionality by deep learning tool in complex nanophotonic designs.

Funding. National Key Research and Development Program of China (2017YFA0205300); National Natural Science Foundation of China (61974069, 62022043); Jiangsu Provincial Key Research and Development Program (BE2018732); Natural Science Foundation of Jiangsu Province (SBK2019020904); NJUPT 1311 Talent Program; NUPTSF (NY219008).

Acknowledgments. L.G. conceived the project, analyzed the data and wrote the manuscript. X.L. and L.J. performed the EM simulations, constructed the NN architecture, analyzed the data and co-wrote the manuscript. Q. W. participated in data analysis and technical discussions. L. W. oversaw and supervised this work.

Disclosures. The authors declare no competing financial interests.

See Supplement 1 for supporting content.

References

1. N. Yu, P. Genevet, M. A. Kats, F. Aieta, J. P. Tetienne, F. Capasso, and Z. Gaburro, "Light Propagation with Phase Discontinuities: Generalized Laws of Reflection and Refraction," Science **334**(6054), 333–337 (2011).
2. S. Sun, K. Y. Yang, C. M. Wang, T. K. Juan, W. T. Chen, C. Y. Liao, Q. He, S. Xiao, W. T. Kung, G. Y. Guo, L. Zhou, and D. P. Tsai, "High-Efficiency Broadband Anomalous Reflection by Gradient Meta-Surfaces," Nano Lett. **12**(12), 6223–6229 (2012).
3. J. P. Balthasar Mueller, N. A. Rubin, R. C. Devlin, B. Groever, and F. Capasso, "Metasurface Polarization Optics: Independent Phase Control of Arbitrary Orthogonal States of Polarization," Phys. Rev. Lett. **118**(11), 113901 (2017).
4. B. H. Chen, P. C. Wu, V. C. Su, Y. C. Lai, C. H. Chu, I. C. Lee, J. W. Chen, Y. H. Chen, Y. C. Lan, C. H. Kuan, and D. P. Tsai, "GaN Metalens for Pixel-Level Full-Color Routing at Visible Light," Nano Lett. **17**(10), 6345–6352 (2017).
5. W. T. Chen, A. Y. Zhu, V. Sanjeev, M. Khorasaninejad, Z. Shi, E. Lee, and F. Capasso, "A Broadband Achromatic Metalens for Focusing and Imaging in the Visible," Nat. Nanotechnol. **13**(3), 220–226 (2018).
6. W. T. Chen, A. Y. Zhu, J. Sisler, Z. Bharwani, and F. Capasso, "A Broadband Achromatic Polarization-Insensitive Metalens Consisting of Anisotropic Nanostructures," Nat. Commun. **10**(1), 355 (2019).
7. X. Chen, L. Huang, H. Muhlenbernd, G. Li, B. Bai, Q. Tan, G. Jin, C. W. Qiu, S. Zhang, and T. Zentgraf, "Dual-Polarity Plasmonic Metalens for Visible Light," Nat. Commun. **3**(1), 1198 (2012).
8. A. Francesco, A. K. Mikhail, G. Patrice, and F. Capasso, "Multiwavelength Achromatic Metasurfaces by Dispersive Phase Compensation," Science **347**(6228), 1342–1345 (2015).
9. X. Ni, S. Ishii, A. V. Kildishev, and V. M. Shalaev, "Ultra-Thin, Planar, Babinet-Inverted Plasmonic Metalenses," Light: Sci. Appl. **2**(4), e72 (2013).
10. S. Wang, P. C. Wu, V. C. Su, Y. C. Lai, Chu. C. Hung, J. W. Chen, S. H. Lu, J. Chen, B. Xu, C. H. Kuan, T. Li, S. Zhu, and D. P. Tsai, "Broadband Achromatic Optical Metasurface Devices," Nat. Commun. **8**(1), 187 (2017).

Optics EXPRESS

11. R. J. Lin, C. V. Wang, S. Su, M. K. Chen, T. L. Chung, Y. H. Chen, H. Y. Kuo, J. W. Chen, J. Chen, Y. T. Huang, J. H. Wang, C. H. Chu, P. C. Wu, T. Li, Z. Wang, S. Zhu, and D. P. Tsai, "Achromatic Metalens Array for Full-Colour Light-field Imaging," Nat. Nanotechnol. **14**(3), 227–231 (2019).
12. S. Wang, P. C. Wu, V. C. Su, Y. C. Lai, M. K. Chen, H. Y. Kuo, B. H. Chen, Y. H. Chen, T. T. Huang, J. H. Wang, R. M. Lin, C. H. Kuan, T. Li, Z. Wang, S. Zhu, and D. P. Tsai, "A Broadband Achromatic Metalens in the Visible," Nat. Nanotechnol. **13**(3), 227–232 (2018).
13. H. M. Yao, M. Li, and L. Jiang, "Applying Deep Learning Approach to the Far-Field Subwavelength Imaging Based on Near-Field Resonant Metalens at Microwave Frequencies," IEEE Access **7**, 63801–63808 (2019).
14. L. Gingras, A. Jaber, A. Maleki, O. Reshef, K. Dolgaleva, R. W. Boyd, and J. M. Menard, "Ultrafast Modulation of the Spectral Filtering Properties of A THz Metasurface," Opt. Express **28**(14), 20296–20304 (2020).
15. N. Papasimakis, Y. H. Fu, V. A. Fedotov, S. L. Prosvirnin, D. P. Tsai, and N. I. Zheludev, "Metamaterial with Polarization and Direction Insensitive Resonant Transmission Response Mimicking Electromagnetically Induced Transparency," Appl. Phys. Lett. **94**(21), 211902 (2009).
16. W. T. Chen, C. J. Chen, P. C. Wu, S. Sun, L. Zhou, G.-Y. Guo, C. T. Hsiao, K.-Y. Yang, N. I. Zheludev, and D. P. Tsai, "Optical Magnetic Response in Three-Dimensional Metamaterial of Upright Plasmonic Metamolecules," Opt. Express **19**(13), 12837–12842 (2011).
17. W. T. Chen, K. Y. Yang, C. M. Wang, Y. W. Huang, G. Sun, I. D. Chiang, C. Y. Liao, W. L. Hsu, H. T. Lin, S. Sun, L. Zhou, A. Q. Liu, and D. P. Tsai, "High-Efficiency Broadband Meta-Hologram with Polarization-Controlled Dual Images," Nano Lett. **14**(1), 225–230 (2014).
18. Y. W. Huang, W. T. Chen, W. Y. Tsai, P. C. Wu, C. M. Wang, G. Sun, and D. P. Tsai, "Aluminum Plasmonic Multicolor Meta-Hologram," Nano Lett. **15**(5), 3122–3127 (2015).
19. R. S. Hegde, "Deep Learning: A New Tool for Photonic Nanostructure Design," Nanoscale Adv. **2**(3), 1007–1023 (2020).
20. J. Jiang, M. Chen, and J. A. Fan, "Deep neural networks for the evaluation and design of photonic devices," ArXiv preprint arXiv. **2007**, 00084 (2020).
21. S. So, T. Badloe, J. Noh, J. Bravo-Abad, and J. Rho, "Deep Learning Enabled Inverse Design in Nanophotonics," Nanophotonics **9**(5), 1041–1057 (2020).
22. Z. Liu, D. Zhu, S. P. Rodrigues, K. T. Lee, and W. Cai, "Generative Model for the Inverse Design of Metasurfaces," Nano Lett. **18**(10), 6570–6576 (2018).
23. Y. Li, Y. Xu, M. Jiang, B. Li, T. Han, C. Chi, F. Lin, B. Shen, X. Zhu, L. Lai, and Z. Fang, "Self-Learning Perfect Optical Chirality via A Deep Neural Network," Phys. Rev. Lett. **123**(21), 213902 (2019).
24. W. Ma, F. Cheng, Y. Xu, Q. Wen, and Y. Liu, "Probabilistic Representation and Inverse Design of Metamaterials Based on A Deep Generative Model with Semi-Supervised Learning Strategy," Adv. Mater. **31**(35), 1901111 (2019).
25. A. M. Hammond and R. M. Camacho, "Designing Integrated Photonic Devices Using Artificial Neural Networks," Opt. Express **27**(21), 29620–29638 (2019).
26. X. Li, J. Shu, W. Gu, and L. Gao, "Deep Neural Network for Plasmonic Sensor Modeling," Opt. Mater. Express **9**(9), 3857–3862 (2019).
27. W. Ma, F. Cheng, and Y. Liu, "Deep-Learning-Enabled On-Demand Design of Chiral Metamaterials," ACS Nano **12**(6), 6326–6334 (2018).
28. I. Malkiel, M. Mrejen, A. Nagler, U. Arieli, L. Wolf, and H. Suchowski, "Plasmonic Nanostructure Design and Characterization via Deep Learning," Light: Sci. Appl. **7**(1), 60 (2018).
29. S. An, C. Fowler, B. Zheng, M. Y. Shalaginov, H. Tang, H. Li, L. Zhou, J. Ding, A. M. Agarwal, C. Rivero-Baleine, K. A. Richardson, T. Gu, J. Hu, and H. Zhang, "A Deep Learning Approach for Objective-Driven All-Dielectric Metasurface Design," ACS Photonics **6**(12), 3196–3207 (2019).
30. J. He, C. He, C. Zheng, Q. Wang, and J. Ye, "Plasmonic Nanoparticle Simulations and Inverse Design Using Machine Learning," Nanoscale **11**(37), 17444–17459 (2019).
31. Y. Kiarashinejad, S. Abdollahramezani, M. Zandehshahvar, O. Hemmatyar, and A. Adibi, "Deep Learning Reveals Underlying Physics of Light–Matter Interactions in Nanophotonic Devices," Adv. Theory Simul. **2**(9), 1900088 (2019).
32. L. Gao, X. Li, D. Liu, L. Wang, and Z. Yu, "A Bidirectional Deep Neural Network for Accurate Silicon Color Design," Adv. Mater. **31**(51), 1905467 (2019).
33. I. Tanriover, W. Hadibrata, and K. Aydin, "A Physics Based Approach for Neural Networks Enabled Design of All-Dielectric Metasurfaces," ACS Photonics **7**(8), 1957–1964 (2020).